Clustering of rRNA operons in *E. coli* is disrupted by σ^H

Khang Ho and Rasika M. Harshey*

Department of Molecular Biosciences and

LaMontagne Center for Infectious Diseases,

The University of Texas at Austin,

Austin, Texas, 78712, USA

* Corresponding author: rasika@austin.utexas.edu

Abstract

Chromosomal organization in *E. coli* as examined by Hi-C methodology indicates that long-range interactions are sparse. Yet, spatial co-localization or 'clustering' of 6/7 ribosomal RNA (*rrn*) operons distributed over half the 4.6 Mbp genome has been captured by two other methodologies - fluorescence microscopy and Mu transposition. Our current understanding of the mechanism of clustering is limited to mapping essential *cis* elements. To identify *trans* elements, we resorted to perturbing the system by chemical and physical means and observed that heat shock disrupts clustering. Levels of σ^H are known to rise as a cellular response to the shock. We show that elevated expression of σ^H alone is sufficient to disrupt clustering, independent of heat stress. The anti-clustering activity of σ^H does not depend on its transcriptional activity but requires core-RNAP interaction and DNA-binding activities. This activity of σ^H is suppressed by ectopic expression of σ^D suggesting a competition for core-RNAP. A query of the other five known σ factors of *E. coli* found that elevated expression of FecI, the ECF σ factor that controls iron citrate transport, also perturbs clustering and is also suppressed by σ^D. We discuss a possible scenario for how these membrane-associated σ factors participate in clustering of distant *rrn* loci.

Introduction

Bacteria inhabit every available niche on earth, where they are subject to a range of environmental conditions to which they must acclimatize [1]. When conditions are favorable, bacteria quickly synthesize proteins required for uptake and biosynthesis of cellular building blocks that enable virtually every aspect of cell growth [2]. The bulk of cellular transcription during this phase is dedicated to *rrn* operons that synthesize ribosomes. Not only are *rrn* operons highly transcribed, but most bacteria also possess multiple such operons. The multiplicity of *rrn* operons has been correlated with elevated growth rate, genome integrity and acquisition of more diverse biosynthetic pathways [3,4], suggesting that there is an evolutionary advantage to maintaining multiple copies of these operons.

There are seven *rrn* operons in *E. coli* (*rrn*A-G), distributed on both arms (replicores) of the bi-directionally replicating chromosome, and residing in the upper half of each replicore [5] (Fig. 1). FROS (Fluorescent Reporter Operator Sites) experiments using pairwise *parS*-ParB interactions showed that 6/7 *rrn* loci spatially co-localize or cluster, reminiscent of the eukaryotic nucleolus [6]. This cluster was not detected by the more widely used Hi-C methodology, which employs formaldehyde to crosslink chromosomal interactions bridged by proteins [7]. Failure to detect the *rrn* cluster by this method could be due to disruption of the cluster by formaldehyde, or to a distance unfavorable for crosslinking. An alternative crosslinking method that exploits the natural mechanism of phage Mu transposition to link distant DNA sites indeed detected the *rrn* cluster [8]. The Mu method is not widely used as yet, because of the limited host-range of Mu, but has been additionally validated by corroborating the existence of a distinct Ter region on the *E. coli* genome [9], as demonstrated using other techniques [7,10].

The FROS study delineated *cis*-acting elements required for *rrn* clustering by systematically deleting regulatory regions upstream of *rrnD* and monitoring its co-localization with

rrnG, both located on the same arm of the chromosome but separated by 700 kbp (Fig. 1) [6]. The study found that clustering required P1, the stronger of the two promoters driving transcription of *rrnD*, as well as an upstream binding site for the NAP (Nucleoid Associated Protein) Fis, but that neither Fis nor other NAPs known to regulate *rrn* transcription were required, suggesting that transcription of the *rrn* locus was not responsible for clustering. Consistent with this notion, mutation of the conserved -10 region of P1 failed to disrupt clustering, indicating that the formation of an open complex was also dispensable. Taken together, these results indicated that multiple transcribing RNA polymerases expected at these highly transcribed loci are likely not the cause of clustering. The Mu method showed that the NAP HUα influenced cluster formation, likely by affecting chromosome compaction in general [8].

To gain more insight into the phenomenon of *rrn* clustering we attempted to perturb the system by subjecting cells to amino acid starvation, as well as to heat, cold and ethanol shock. Of these, heat shock completely disrupted clustering. The heat shock response, part of the more general unfolded protein response [11], is designed to maintain heat-denatured proteins in a properly folded state, a key player in this response being σ^H [12]. σ^H (RpoH) regulates a large number of genes, notably those encoding protein chaperones such as GroEL/GroES [13,14]. We show that it is the rise in σ^H levels and not heat stress *per se*, that disrupts clustering and corroborate this observation using the Mu method. The observed σ^H-promoted de-clustering could be counteracted by simultaneous expression of σ^D (or σ^{70}). A similar but weaker effect on de-clustering was exhibited by FecI, which was also rescued by σ^D. Both σ^H and FecI are associated with the inner membrane. Based on these findings, we propose a model for how clustering of *rrn* operons occurs at the membrane and might be driven by the ability of sigma factor(s) to assemble RNAP onto cognate promoters.

Results

Heat shock disrupts *rrnA-rrnD* clustering

Gaal et al. used FROS to examine pair-wise combinations of fifteen of the possible twenty-one pairs of *rrn* operons, using distinct *parS*-ParB partners derived from phage P1 and plasmid pMT1 of *Yersinia pestis* (Fig. S1) [6,15]. In this study, we employed the same approach to determine *trans*-acting factors involved in clustering (Fig 2A). For our analysis we chose *rrnA* and *rrnD*, located on two different replicores (Fig. 1), directing ParB-GFP 361bp upstream of *rrnA* and ParB-CFP 282 bp upstream of *rrnD* by inserting their respective *parS* sites at these locations (Fig. 2A); median *rrnA-D* distance was estimated to be 134 nm. These cells were then subjected to various well-studied chemical and physical stresses (Fig. 2B). Serine hydroxamate (SHX) is a serine analog that inhibits $tRNA^{ser}$ aminoacylation, mimicking amino acid starvation and inducing a stringent response with concomitant synthesis of (p)ppGpp [16,17]. Application of this stress failed to produce a notable change (>2-fold) in the median *rrnA-D* distance (214 nm, compared to a significance cutoff at 230 nm; see figure legend for assignment of significance). Cold shock, which elicits changes in membrane fluidity, protein and nucleic acid folding and ribosome assembly [18], also did not significantly perturb clustering (216 nm). Ethanol damages cell wall and membrane integrity, inducing an unfolded protein response in addition [11,19]. This stress increased the *rrnA-rrnD* distance to 424 nm. The unfolded protein response can also be produced by heat stress, which produced the most pronounced shift of the median distance relative to control (734 nm) (Fig 2B). Representative images from these experiments are shown in Figure 2C-D. We note that heat stress appears to localize *rrnA*, but not *rrnD*, to the pole, while also reducing the number of *rrnA* loci to 1 (Fig 2D, green arrow). Since ethanol also induces the unfolded protein response, we infer that it is the unfolded protein response that promotes de-clustering of *rrnA* and *rrnD*.

Since our laboratory has shown that long-range contacts occur less frequently in an *hupA* (HUα) mutant [8], we also examined a noncoding (nc) RNA known to interact with HU [20]. A

single deletion of nc5 showed no difference in the median distance between *rrnA* and *rrnD* (Fig. S2). RpoZ (an RNAP subunit) and NusB (a component of the anti-termination complex that interacts with RNAP), reported to contribute to phase-separation of *E. coli* RNAP [21], were also examined. Deletion of either *rpoZ* or *nusB* elicited a small increase (i.e. above our 2-fold cutoff of 230 nm) in the *rrnA-D* distance (254 nm and 304 nm, respectively) (Fig S2), but not as drastic as that of heat stress.

In summary, of all the variables tested, heat stress caused the most significant de-clustering of the *rrnA-D* pair, followed by ethanol stress. These two stresses share the common outcome of producing an unfolded protein response.

Deregulation of GroEL/S disrupts *rrnA-rrnD* clustering

Since heat shock disrupted the *rrnA-D* pair, we hypothesized that some protein factor(s) bridging the two loci was displaced as a result. To identify bound proteins, we directed dCas9 (a variant of Cas9 capable of binding but not cleavage [22]), to upstream regions of all seven *rrn* loci, similar to the location of *parS* sites (see Table S2), using the appropriate gRNAs. dCas9 was fused to 3X-FLAG, so anti-FLAG antibodies were used in pulldown experiments (Fig. 3A). The efficiency of sgRNA targeting was determined by assessing lethality when Cas9 was provided instead of dCas9 (Fig. S3). Overall, in a host expressing Cas9, sgRNAs directed to all *rrn* operons caused a reduction in viability relative to a no-PAM control (Fig. S3). The differences in gRNA efficiency may influence the efficiency of dCas9 pulldowns, but since Cas9 targeting was productive, we concluded that the pulldowns would reflect at least the binding of dCas9 to the rDNA.

Mass spectrometry of the proteins identified in pull-downs with the seven *rrn* samples showed a range of significantly enriched proteins across different sgRNAs (z-score> 2.5, computed from three biological replicates for each sgRNA) using the methods described in [23]. Common

proteins identified across multiple samples are summarized in Fig. 3B. For sgRNA targeting *rrnA, rrnB, rrnC, rrnD, rrnE, rrnG,* and *rrnH*, we found 54, 132, 135, 105, 66, 33 and 107 significantly enriched proteins, respectively (Fig. 3C and Fig. S4). The detailed spectral counts of identified proteins for each sgRNA can be found in Tables S3-S9. No common protein was significantly enriched across all samples, but GroEL was enriched in 4/7 sgRNAs (*rrnC, rrnA, rrnB,* and *rrnD*), suggesting that GroEL could be a possible *trans*-acting factor in clustering.

GroEL, in complex with GroES, acts as a chaperone for protein folding [24]. To investigate whether GroEL mediated *rrn* clustering, we generated a chromosomal *groEL* deletion in the *parS*-tagged *rrnA-D* strain (Fig. 3D). Since *groEL* is essential [25], we provided it in *trans* from a plasmid under control of pAraBAD and verified induction (with arabinose) and repression (with glucose) by observing corresponding increases and decreases in colony sizes, respectively (Fig S5). Examination of the degree of *rrnA-rrnD* clustering under these two conditions showed that clustering was disrupted with arabinose addition (Fig. 3, third plot from the left), even though GroEL levels were sufficient for growth as judged by colony size (Fig. S5); the median distance between *rrnA-D* increased to 494 nm. A WT 'control' carrying both *groEL*/*groES* under pAraBAD control increased *rrnA-D* distance to 216 nm (Fig. 2D, second plot from left); this slight increase is not significant based on our 2-fold cut-off, but the data nonetheless suggest that ectopic expression *of groES/EL* affects clustering. Taken together, these results suggest that any perturbation of normal GroES/EL levels destabilize clustering. Since these two genes are co-transcribed [26], we wondered if the imbalance in their relative levels was responsible for cluster disruption. We therefore placed the entire *groES/EL* operon on the plasmid vector in the Δ*groEL* strain, but that did not restore clustering either (Fig. 3D, rightmost plot).

To test if expression of *groES/groEL* from their native σ^H-promoter (pGroE) would change the results, we compared *rrnA-D* distance when expression of this operon was controlled by pGroE vs pAra in both WT and Δ*groEL* strains (Fig. 4E). A shift closer to normal in the *rrnA-D* distance

as indicated by the 25% quartile of 242 nm for pGroE vs 356 nm for pAra (Fig 3E, compare rightmost two plots), suggests that transcription from the native promoter was better at restoring clustering. σ^H, also known as σ^{32} or RpoH, is the major heat shock sigma factor that transcribes the *groEL/S* operon exclusively [26]. Its levels are kept low through multiple mechanisms, including sequestration at the inner membrane, and direct interaction of GroEL/ES with σ^H [27,28]. Could our inability to restore *rrnA-rrnD* clustering in the Δ*groEL/ES* background be attributable to perturbation of σ^H levels? This was tested next.

σ^H disrupts *rrnA-rrnD* independent of its transcriptional activity

If perturbation of σ^H was the cause of *rrnA-D* de-clustering, we hypothesized that ectopic expression of σ^H alone should give similar results. We therefore placed *rpoH* under an inducible Tet promoter (pTc). Consistent with our expectations, *rpoH* induction increased the median distance between *rrnA-D* to 566 nm (Fig 4A, third plot from left). However, the same result was seen even in the absence of *rpoH* induction (Fig. 4A, second plot from left). To verify that *rpoH* was being expressed from the plasmid, we constructed a *lacZ* reporter driven from p*htpG*, a weak σ^H-responsive promoter [29], and assessed *lacZ* expression upon induction of *rpoH* from pTc (Fig 4B). A small but significant increase in β-galactosidase activity was observed after an hour of induction, the same time frame employed for microscopy (Fig. 4A), indicating that *rpoH* was expressed from the Tet promoter. We conclude that even a small increase in σ^H levels promotes de-clustering of *rrnA-rrnD*.

E. coli possesses seven experimentally confirmed sigma factors, of which the vegetative σ^D (RpoD or σ^{70}) is the most abundant [30]. Since the amount of RNAP is thought to be relatively constant across most growth conditions, competition among the sigma factors for this core RNAP has been proposed to be the mechanism for gene regulation [30,31]. To test if competition

between σ^H with σ^D for binding RNAP could be responsible for destabilizing clustering, we inserted *rpoD* downstream of TetR on the same plasmid, which is driven by the constitutive promoter divergent from pTc (pTetR). Expression of *rpoD* decreased the median distance between *rrnA-D* to 213 nm compared to 566 nm with the *rpoH* vector alone (Fig 4A, compare fourth plot to second plot from the left), supporting the notion that competition between σ^D and σ^H for core RNAP likely suppressed the de-clustering activity of σ^H.

To test this notion further, we examined the following previously characterized mutants of *rpoH,* reported to have decreased or increased transcription activities: L245P is defective for interaction with RNAP [32], E265A is defective for promoter binding at the -35 region [32], and I54N has increased stability [28,29] . Our expectation was that the L245P and E265A would lose their de-clustering activity, while I54N mutant would not. This expectation was borne out for the L245P and E265A variants (303 nm and 216 nm, respectively), but not for I54N (284 nm) i.e. all three variants were defective in destabilizing the *rrn* cluster, compared to WT RpoH (566 nm) (Fig 4C). We note that in contrast to cells expressing the first two variants, those expressing I54N are elongated (Fig S6). I54N has been shown to exhibit elevated transcriptional activity due to its inability to localize to the membrane like WT σ^H [27,29], which likely perturbs normal cell physiology. The expected transcriptional activity of all the σ^H mutants was confirmed using the *lacZ* reporter as before (Fig. 4D). We conclude that σ^H-mediated de-clustering is independent of its transcriptional activity.

σ^H does not disrupt all *rrn* pairs

Our experiments thus far queried the co-localization of the *rrnA-rrnD* pair as representative of all the *rrn* loci found in the cluster [6]. To test if heat shock and σ^H were equivalent in their disruptive ability, we decided to query other pairs, including every co-localizing *rrn* operon at least once, with *rrnC* as the non-clustering control. Heat shock disrupted clustering of all non-C *rrn* operons tested,

the median distance increasing 1.5 - 2.5 fold (from 80-120 nm to 450-700 nm) (Fig 5A; summary of the results diagrammed in Figure 5B). *rrnC* is reported to not be part of the cluster [6,8], yet its distance from *rrnG* remained curiously unperturbed by heat, staying at ~400nm median, suggesting perhaps a specificity to clustering that supersedes the global unfolding effect of heat stress.

The effect of σ^H on the *rrn* pairs tested was non-uniform (Fig. 5C). Specifically, we observed that two pairs that shared *rrnH* appeared to be resistant to disruption by σ^H (Fig 5C). Thus, contacts between all the *rrn* loci in the cluster are not uniform, suggesting that there is likely a sub-organization within this structure.

To determine if σ^H played a unique role in affecting cluster stability, we ectopically expressed the other five sigma factors: RpoE (σ^{24}), RpoF (σ^{28}), RpoN (σ^{54}), RpoS (σ^{38}) and FecI (σ^{19}), under the same promoter as the *rpoH*-expressing vector, maintaining the same RBS (ribosome binding site). Of these, FecI produced a smaller destabilizing effect (84 nm vs 234 nm for RpoH) (Fig. 5D). To test if σ^D would restore clustering to the FecI-expressing strain like it did when co-expressed with σ^H (Fig. 4A), we co-expressed *rpoD* with *fecI*; clustering was completely restored wild type levels (Fig. 5D, compare last two plots). We note that the shared properties of RpoH and FecI are that they are both normally sequestered at the inner membrane, suggesting perhaps that *rrn* clustering may have a membrane component.

σ^H disrupts the *rrn* cluster as tracked by the Mu method

Phage Mu transposition requires direct contact between Mu and its transposition target and displays virtually no sequence specificity in its target choice [33]. Higher or lower frequencies of transposition are therefore interpreted to reflect higher or lower rates of physical contact between the interacting chromosomal regions, analogous to the contact frequencies inferred from normalized Hi-C data [34]. Contacts made by Mu when located next to *rrnD* showed significantly

positive interaction between *rrnD* and chromosomal regions containing the *rrnA, B, E, G, and H* (but not *rrnC*), suggesting physical proximity of these regions, as also seen by FROS [6].

Since we did not examine the effect of σ^H on all possible combinations of *rrn* loci with FROS (Fig. 5), we used the Mu method to examine transposition patterns of Mu located near *rrnD* in the presence of ectopically expressed RpoH. The pattern of Mu transposition from the *rrnD*-proximal locus in WT cells was consistent with the earlier report, where Mu could access every region of the chromosome irrespective of its starting location (Fig 6A). In the presence of the vector encoding RpoH, even without induction of RpoH expression, the transposition landscape was altered, with more Mu insertions now occurring proximal to the starting Mu in Bin 72 (Fig 6B). This increase in local versus distal contacts is not exacerbated with *rpoH* induction (Fig 6C), similar to microscopy data (Fig. 4A). Transposition frequencies across different conditions are summarized in Fig 6D. Even though Mu insertion frequency at its starting bin is the highest across all conditions, in the presence of *rpoH* overexpression, a global decrease is seen in the non-starting bins (RpoH and +RpoH column compared to None column), indicating that *rpoH* overexpression disrupts long-range contacts.

We next examined specifically the bins containing *rrn* operons to assess the effect of RpoH on Mu transposition. We observed that contact between *rrnD* and a majority of the *rrn* loci decreased, with the notable exception of those with *rrnC* and *rrnH*, which remain unchanged (Fig. 6E). The *rrnC* result is consistent with earlier reports [6,8], and the *rrnH* result is consistent with data in Figure 5C, where RpoH promoted de-clustering of all *rrn* examined, with the exception of *rrnH*. Overall, Mu transposition data support the hypothesis that σ^H promotes de-clustering of *rrn* operons.

Discussion

This study demonstrates that the *E. coli* 'nucleolus' where 6/7 *rrn* operons are reported to co-localize, can be perturbed by the cellular heat shock response as demonstrated by both FROS and Mu transposition. This perturbation is not due to heat stress per se, but rather due to elevation of RpoH or σ^H levels known to occur during the response. We discuss below what this and other data may suggest about the mechanism of co-localization of the *rrn* operons.

Ability to disrupt its organization validates the existence of the *E. coli* 'nucleolus'

In eukaryotic cells, the nucleolus is the primary site of ribosome biogenesis [35]. It is a large structure, where hundreds to thousands (depending on the organism) [36], a device thought to have evolved to maximize translation efficiency [35]. By contrast, *E. coli* has only seven operons encoding ribosomal DNA (*rrn* operons) [37] (Fig. 1). That 6/7 of these operons come together is some as-yet unknown fashion was first reported by Gaal et al. using FROS methodology, who called this organization a 'bacterial nucleolus' and showed that its presence was independent of growth media and of cell doubling times [6]. A completely different Mu methodology detected the proximity of the same 6/7 *rrn* operons [8], providing strong support for this observation.

Gaal et al. found that the only *cis* elements required for formation of the *E. coli* nucleolus were the P1 promoter and an UP element that contained FIS binding sites in one of the interacting *rrn* pairs tested (Fig. 1). However, neither Fis nor active *rrn* transcription was required, as gleaned from recalcitrance of the *rrn* cluster to disruption by addition of rifampicin, which stops RNA chain elongation [38], as well to mutation of a -10 region in the P2 promoter that prevents open complex formation that signals initiation of transcription. These properties of the *E. coli* nucleolus are in contrast to the requirement for Pol I function and rRNA transcription to maintain nucleolar structure and integrity in eukaryotic cells [39]. We will therefore simply call this co-localization an *rrn* cluster.

To learn more about the nature of the *rrn* cluster, we attempted to perturb it by exposing cells to several environmental stressors (Fig. 2B). Of these, heat and ethanol shock had the largest effect. These two stressors share a common 'unfolded protein' response [11]. The important take-away from this experiment is that by perturbing the cluster, we had not only validated its existence but found a handle to probe its nature.

The heat shock response, GroEL/GroES and σ^H all destabilize the *rrn* cluster: σ^D counteracts the action of σ^H

Adaptation to heat shock is a universal biological phenomenon [11]. Heat denatures proteins, so organisms adapt by synthesizing protein-folding chaperones. *E. coli* encodes several chaperones including GroEL/GroES and employs σ^H to transcribe hundreds of genes that enable bacterial survival [13,14]. The ability of heat shock to disrupt the *rrn* cluster suggested to us that proteins must participate in holding the structure together at some level. We therefore directed FLAG-tagged dCas9 immediately upstream of each of the 7 *rrn* loci, followed by pull-down with FLAG antibodies and mass spectroscopy. No common protein was significantly enriched across all samples, but GroEL was enriched in 4/7 sgRNAs (*rrnC, rrnA, rrnB,* and *rrnD*), suggesting that GroEL could be a possible *trans*-acting factor in clustering (Fig. 3A-C; Fig. S4). (Although *rrnC* is not part of the cluster, it is close to the origin of replication *ori*, and it is conceivable that unrelated events at *ori* block its incorporation into the cluster).

To query the participation of GroEL directly, we attempted to delete the chromosomal copy of this essential gene while providing it ectopically from either a regulated promoter or its native promoter. Both manipulations disrupted the *rrn* cluster, although expression from its native promoter was slightly less disruptive (Fig. 3E). The *groEL/S* operon is transcribed exclusively by the major heat shock sigma factor σ^H, whose levels are kept low through multiple mechanisms,

including sequestration at the inner membrane where it is degraded by protease FtsH, as well as direct interaction with GroEL/ES [27,28]. To test if our manipulations of GroEL were perturbing σ^H levels, we provided RpoH ectopically from a regulatable promoter. Even in the absence of induction, leaky expression of RpoH was sufficient to disrupt the *rrn* cluster (Fig. 4A).

Why should an apparently slight rise in σ^H levels have such a profound effect on stability of the cluster? Given that the P1 promoter and its UP elements participate in maintaining the cluster, we imagined a scenario where RNAP bound to the housekeeping σ^D, known to transcribe the *rrn* operons [5], was stationed there and that σ^H might be competing with it for binding RNAP, displacing it and disrupting the structure. We tested this conjecture by inserting *rpoD* along with *rpoH* on the ectopic vector. This resulted in significant cluster rescue compared to *rpoH* alone (Fig 4A), supporting our conjecture.

Sigma factors that disrupt the *rrn* cluster associate with the membrane, suggesting a model for *rrn* clustering

RNAP levels in *E. coli* are constant, so competition among the sigma factors for the core RNAP has been proposed to be the mechanism for gene regulation [31]. This competition model predicts that mutants of σ^H that are defective for either RNAP-core or DNA-binding should not disrupt the cluster. We tested this by querying two RpoH mutants, one defective for interaction with RNAP and the other defective for promoter binding at the -35 region. Both mutants were significantly deficient in the de-clustering activity of WT RpoH (Fig. 4C), in keeping with the competition model.

σ^H levels are regulated by at least three mechanisms: control through GroEL/GroES, DnaJ/K/GrpE, control of translation efficiency at the mRNA level, and the degradation of σ^H by FtsH, an integral-membrane protease. A third RpoH mutant we tested for its de-clustering activity was I54N, shown to escape FtsH-mediated proteolysis through the inability of the SRP (Signal

Recognition Particle)-ffh complex to recognize a patch of amino acids between domain 1 and domain 2 of RpoH, which would result in its being trafficked to the inner-membrane for degradation by FtsH. Our expectation was that this mutant would behave like WT RpoH. Despite its high transcription activity (Fig. 4D), however, the effect of the I54N mutant did not align with our expectations (Fig. 4C), showing at the very least that high levels of transcription directed by σ^H are not the cause of de-clustering, and that none of the members of the σ^H regulon are involved in de-clustering. So why did the I54N mutant not behave like WT RpoH? Unlike the WT protein, I54N mutant is unable to localize to the membrane, suggesting that access to the membrane is important for the de-clustering effect of RpoH, ergo, the *rrn* cluster might be anchored in the membrane.

When we tested the cluster-disrupting ability of five other sigma factors - RpoE (σ^{24}), RpoF (σ^{28}), RpoN (σ^{54}), RpoS (σ^{38}) and FecI (σ^{19}) - we found that that FecI, an extracytoplasmic-function (ECF) σ factor, also disrupted clustering, although not as severely as σ^H (Fig. 5D). FecI, along with FecA and FecR, is responsible for the transcription of the ferric citrate transport system, consisting of *fecABCDE* transport genes [40]. FecA is an outer membrane protein that transports $(Fe^{3+}\text{-citrate})_2$ across the outer membrane. Upon binding of $(Fe^{3+}\text{-citrate})_2$ to FecA, the signal is then transduced through the periplasmic face of FecR, an inner membrane protein, to its cytoplasmic face [41,42]. This conformational change of FecR activates the transcriptional activity of FecI in the cytoplasm and promotes transcription of *fecABCDE* [43]. The dependence of FecI on FecR, which is localized to the inner-membrane, for efficient transcription by RNAP-FecI of the *fec* operons, also lends support to a model where the site of *rrn* clustering is the inner membrane.

In contrast, overexpression of σ^E, which is also an ECF, failed to disrupt clustering [44,45]. The mode of regulation of σ^E is based on the repression of σ^E by the inner membrane anti-sigma factor RseA, which is sandwiched between domain 2 and domain 4 of σ^E, thereby inhibiting the interaction of RNAP core and σ^E [46,47]. Upon membrane stress, such as ethanol or heat, DegS

is activated by the presence of unfolded outer-membrane proteins, and, in concert with RseP, degrades RseA, releasing σ^E to promote transcription of downstream genes [48,49]. The negative regulation by RseA may explain why overexpression of σ^E alone is unable to disrupt clustering. In other words, for efficient disruption of the *rrn* cluster, σ^D-independent transcription needs to occur at the inner membrane.

Taken together, we propose that clustering of *rrn* is mediated by σ^D at the membrane either through σ^D directly or through other unknown factor(s) (Fig. 7). σ^D has indeed been observed at the membrane [28]. Given that high levels of transcription are not required, but the *cis*-acting elements responsible for high transcriptional activity of *rrn* are, and that some σ factors can disrupt clustering implicating σ^D as the clustering factor, we propose that the assembly of RNAP holoenzyme and UP element features of P1 drives *rrn* clustering. Upon heat stress or elevated σ^H levels, RNAP complexes bound to σ^D are displaced through competition with σ^H, and to a lesser extent FecI, for RNAP core, resulting in de-clustering of *rrn* operons. The order of RNAP assembly has been shown to be $\alpha_2 \rightarrow \beta \rightarrow \beta' \rightarrow \sigma$ [50] or $\alpha_2 \rightarrow \beta \rightarrow \beta' \omega \rightarrow \sigma$ [51]. The requirement for the P1 promoter may reflect the high affinity of α for the UP element present upstream of the -35 element [52]. The dimerization of the α subunit could drive the bridging interaction between the disparate *rrn* operons. However, this interaction by itself is unable to explain *rrn* clustering as demonstrated by de-clustering effect of σ^H and FecI, since σ factor binding and unwinding of the DNA duplex is the last step of RNAP assembly. Therefore, we propose that two elements are responsible for *rrn* clustering: (1) the high affinity of α for the UP element, and (2) DNA binding driven by σ^D. The affinity of α for the *rrn* UP element would explain why *rrn* clustering does not extend to other non-*rrn* loci. The specificity of σ^D for the *rrn* promoter would explain the de-clustering activity of σ^H and FecI. We note that σ^H did not affect the position of two pairs that shared *rrnH* (Fig 5C), suggesting a likely a sub-organization within this structure. Finally, why did we recover GroEL at 4/7 rDNA loci (Fig. 3A-C and Fig. S4)? One possibility is that GroEL is meant

to clear σ^H from the cluster [27]. Alternatively, since GroEL has been shown to restore transcription of heat-treated RNAP *in vitro* [53], it could either be interacting non-specifically with some component of RNAP or ensuring that the proteins at the cluster do not aggregate.

Relationship of the *rrn* cluster to RNAP condensates

RNAP has been reported to form distinct clusters on the *E. coli* nucleoid [54,55]. Since the bulk of cellular transcription is dedicated to rRNA transcription and since RNAP clusters form in fast-growth conditions, it was proposed that these clusters represent high concentrations of RNAP on *rrn* operons [56]. Subsequent work showed that RNAP clusters colocalize with nascent rRNA, but that their spatial arrangement was not dependent on rRNA synthesis activity and was likely organized by the underlying nucleoid [57]. RNAP clusters have been shown to be biomolecular condensates capable of phase separation, involving known factors associated with RNAP (i.e. ω subunit of RNAP, and NusB) [21].

The properties of the *rrn* cluster are on the one hand reminiscent of RNAP condensates in that high level of transcription of rRNA is not required for their organization, but, on the other hand, are different in that the cluster is immune to transcription inhibitors while the condensates are not [57]. For example, neither treatment of transcriptional inhibitor Rifampicin (Rif) nor SHX, which inhibits rRNA transcription through the formation of (p)ppGpp, disrupts the cluster [6]. The cluster is unlikely to serve as a precursor for formation of RNAP condensates since these form in a strain where only one *rrn* operon is present [48]. Antitermination factors such as NusB and ω subunit of RNAP have been shown to contribute to formation of RNAP condensates [23]. However, we showed in this study that neither Δ*nusB* nor Δ*rpoZ* strains significantly impact the cluster (Fig. S2). We interpret these results to mean that RNAP condensates represent a feature

of highly active transcription that the *rrn* cluster contributes to by making rDNA readily available through spatial localization.

Acknowledgments

We thank Rick Gourse for providing pFHC2973, and *parS*-labelled *rrn* strains, Ian Molineux for providing the parent strain that supports replication of R6K origin plasmids, Kamyab Javanmardi for providing Golden Gate vector for gRNA insertion, Rachael Cox and Edward Marcotte for script and computing power used in mass spectrometry analysis, Lydia Freddolino for suggesting use non-Mu reads to correct for replication effects, and Brady Wilkins for assistance with Southern Blot. This work was supported by NIH grant GM118085.

Materials and Methods

Media, Strains, Phages and Plasmids. Unless conditions are specified, all strains are grown in LB at 30°C with shaking. When appropriate, antibiotics were at the following concentrations: Ampicillin (Amp) at 100μg/mL, Kanamycin (Kan) at 25μg/mL, Chloramphenicol (Cam) at 20μg/mL. Anhydrotetracycline (aTc) was used for induction of Tet promoter at 50ng/mL. Isopropyl-β-D-Galactoside (IPTG) was used to induce the *lac* promoter at 1mM. o-nitrophenyl-β-D-Galactoside (ONPG) was purchased from Sigma. Competent cells for transformation were prepared by washing a growing culture of O.D. 0.4-0.5 in cold 10% glycerol 3 times. The pellet was resuspended in 1:100 of the original volume in 10% glycerol. Electroporation was performed in *E. coli* Pulser (Biorad) with 1mm Electroporation cuvette Plus (Fisher) at 1.8V. Cells were recovered in SOC (LB supplemented with 10mM $MgCl_2$, 10mM $MgSO_4$, and 0.2% Glucose) for 1.5 hours at 30°C with shaking prior to plating on the appropriate selection. Mu phage was stored in Mu Buffer

(50mM Tris-HCl pH 8.0, 100mM NaCl, 5mM $CaCl_2$, 5mM $MgCl_2$, and 0.1% gelatin). Strains and Phages employed in this study are listed in Table S1. Primers, purchased from Integrated DNA Technology (IDT), used in this study are listed in Table S2.

General Molecular Techniques. Routine PCR were performed with Taq DNA Polymerase (NEB), according to manufacturer's instructions. PCR fragments for cloning were generated with Phusion DNA Polymerase (NEB) according to manufacturer's instructions. Gibson Master Mix was made according to Gibson *et al* [58]. Gibson assembly was performed at 50°C for at least 2 hours. Golden Gate Assembly was performed with Esp3I (NEB), T7 DNA Ligase (NEB), T4 DNA Ligase Buffer (NEB). Primers used to generate the gRNA were used at 10nM each. 100ng of the destination vector was used. The program for Golden Gate Assembly was 3 minutes at 37°C, 2 minutes at 16°C for 35 cycles, followed by 1 cycle of 10 minutes incubation at 37°C. T4 DNA Ligase, T4 PNK, and T4 DNA Ligase Buffer were purchased from NEB.

Plasmid Construction. Plasmids were constructed using Gibson assembly. Typically, 250µL of the backbone was assembled with a molar equivalent of insert in a 20µL reaction. The resulting product was purified with PCR clean-up kit (Qiagen) according to the manufacturer's instructions. 2µL of the 20µL eluted product was used for transformation. Colonies were screen by PCR with primers spanning the junction between the backbone and the insert. Positive clones were restruck and checked once more using the same primer pairs. The PCR product was sequenced to confirm the identity of the sequence at either the UT Core Sequencing Facilities or Eton Biosciences. For generating single point mutants, primers carrying the desired mutation were used to amplify the plasmid of interest. The resulting PCR product was gel-extracted with Qiagen Gel Extraction Kit. The product was then self-ligated overnight with T4 DNA Ligase and T4 DNA PNK in T4 Ligase Buffer. The ligated product was then purified and 2µL of the 20µL eluted product was used for transformation. Positive clones carrying the desired mutation were identified by PCR of the target

sequence followed by sequencing. The positive clones were then restruck once again and verified with PCR and sequencing.

Strain Construction. For insertion of *parS* sequences, the procedure was essential was described in [59] with the exception being the template plasmid (pKH3 or pKH4) carrying the appropriate *parS* linked to antibiotic resistance cassette. Briefly, 0.5mL of an overnight culture of MG1655 carrying pKD46 was pelleted, washed twice in 1mL of PBS, and diluted 1:100 in fresh LB supplemented with 0.2% arabinose. The culture was grown to an O.D. of approximately 0.4. The cells were made electrocompetent. Cells were then transformed with the appropriate PCR product and let recover in SOC for 3 hours at 30°C. The outgrowth was then plated on the appropriate selection and incubated at 37°C overnight. Positive clones were identified by PCR with primers amplifying the junction of expected insertion. Positive clones were struck out on the appropriate selection plate at 37°C and reconfirmed with PCR followed by sequencing. To remove the antibiotic-encoding cassette for subsequent insertion of additional *parS*, pCP20 was transformed into the desired host strain. Clones carrying pCP20 were then struck out on LB plate without selection and incubated at 42°C overnight. Colonies were then checked for the loss of both pCP20 and the antibiotics cassette by streaking on the appropriate selection.

Fluorescent Microscopy and Post-Processing. Overnight cultures used for fluorescent microscopy were grown overnight in EZ-Rich media (Teknova) from single colony and diluted 1:100 in fresh EZ-Rich media supplemented with IPTG for induction of ParB-fluorescent fusions from pFHC2973. The subculture grew until an O.D. of 0.4. 1mL of the culture was then pelleted by centrifugation and resuspended in 100µL of PBS. 6uL of the suspension was then spotted onto agarose pad (1%) and let dry. The sample was then observed under Olympus-XM10 camera 100x objective with oil immersion. Most images were taken at an exposure of ~100ms for GFP filter, and ~400ms for CFP filter, however, some samples required a longer exposure time to obtain acceptable signal for downstream processing; the upper limit of exposure was 3s. Cellular

stressors were applied 20 minutes prior to imaging, after which they were prepared and imaged as described above. For heat stress, the cells were transferred to a 42°C water bath. SHX was added to a concentration of 50μM. Cold stress was 4°C water bath. Ethanol stress was induced by adding ethanol to 0.5%. For image-processing, the background was subtracted from the image, and foci were detected with ImageJ using the detect maxima function. The coordinates of the foci were exported and the Cartesian distance between a GFP focus, and its closest CFP focus was determined with custom Python script. The distance was computed by scaling the distance in pixel to nm with 1 pixel = 62nm. Due to the large number of foci observed, even datasets that produced small differences in the median distance would be statistically significant. We therefore arbitrarily determined that a 2-fold change in median distance is significant.

Pulldown of dCas9 and Proteomics. Three independent overnight cultures of MG1655 carrying pKH5 and the corresponding gRNA were pelleted and washed as described above. The pellet was diluted 1:100 into 100mL fresh LB supplemented with selection and 0.2% arabinose and aTc. The cultures were grown to an O.D. of 0.6 and pelleted and washed 3 times in 1mL of PBS. The subsequent pulldown procedure was carried out as described by FLAG Immunoprecipitation kit (Rockland). Every step of the pulldown was conducted at 4°C. Briefly, the pellet was resuspended in 5mL of lysis buffer and sonicated (Brason tip, 40% intensity) for 10 minutes (10s on, 10s off cycle). The lysate was clarified by centrifugation at 4°C. Agarose-αFLAG Ab was washed twice in PBS and once in elution buffer. The washed Agarose-αFLAG Ab was incubated with the lysate overnight. After incubation, the beads were collected and washed 3 times with PBS. The bound proteins were eluted with elution buffer. The proteins were quantified by Mass Spectrometry at the UT Proteomics core. Samples were digested with trypsin, desalted and run on Dionex LC (liquid chromomatography) and Orbitrap Fusion 2 (mass spec machine) for 60 minutes. Raw data were analyzed with PD2.2 and Scaffold 5 software. Downstream analysis was performed as

488 described in [23] with lacZ gRNA pulldown as the negative control. Significantly enriched hits were
489 ranked based on a z-score cut-off of 2.5.

490 **Miller Assay**. 0.5mL of three overnight cultures of desired strain carrying the appropriate plasmid
491 was pelleted and washed in 1mL of PBS twice. The pellet was then resuspended in 0.5mL of PBS
492 and diluted 1:100 in LB. The cultures were grown to an O.D. of 0.4 and aTc was added. At
493 indicated time points, 20µL of the culture was withdrawn, its O.D. 600 recorded and added to
494 80µL of permeabilization buffer (100mM $NaHPO_4$, 20mM KCl, 2mM $MgSO_4$, 0.8mg/mL CTAB,
495 0.4mg/mL sodium deoxycholate, 5.4µL/mL β-mercaptoethanol). After the final time point, 600µL
496 of substrate solution (60mM Na_2HPO_4, 40mM NaH_2PO_4, 1mg/mL ONPG, 2.7µL/mL β-
497 mercaptoethanol) was added to each sample. The samples were incubated at 30°C for 60
498 minutes before 600µL of 1M Na_2CO_3 was added to stop the reaction. O.D. 420 was recorded.
499 Miller units were calculated as follows:

500 $$Miller\ Units = 1000 \times \frac{Absorbance_{420nm}}{60 \times Absorbance_{600nm} \times 0.02}$$

501 **Mu Phage Preparation.** When required, lysogen of the indicated prophage was grown overnight,
502 diluted 1:100 in fresh LB and grown until an O.D. of 0.5. After which, the culture was shifted to a
503 42°C waterbath and incubated until lysis is complete. The lysate was clarified by centrifugation at
504 6000g for 20 minutes. The supernatant was transferred to a clean flask and NaCl was added to
505 a final concentration of 0.5M followed by the addition of Polyethylene glycerol 8000 to a final
506 concentration of 10% w/v. The mixture was incubated overnight at 4°C. The pellet was then
507 collected by centrifugation at 8000g for 20 minutes. The pellet was then resuspended in 1:100 of
508 the original volume in Mu Buffer. Chloroform was added to the mixture and shaken. The phases
509 were separated by centrifugation at 4000g for 10 mins at 4°C. The aqueous phase was collected
510 (top layer) and titered prior to use.

Generation of mlaF::Mu and single-transposition experiments. Selection for Mu insertion at *mlaF* (bin72 as described in [8]) was performed by first introducing *sacB* at *mlaF* followed by infection Mu carrying a Cam marker. Briefly, *attP* was introduced into *mlaF* by λred recombination, and the Kan marker was removed. KH2 was then introduced into this strain, induced for expression of λ Int with arabinose followed by transformation of KH22. Clones positive for integration of the *sacB-kanR* cassette was verified by PCR spanning the expected junction between the cassette and *mlaF*. This strain was then infected with Mu::Cam at an MOI of 5, and survivors that were resistant to sucrose and Cam were selected for. Three colonies were picked and insertion locations for each were confirmed with PCR. Southern Blot was performed to confirm that only one Mu inserted. Of 3 clones picked, one was confirmed to be a mono-lysogen. This strain was designated KH10. Single hop experiment performed with KH10 was performed as described in [8] with modifications for plasmid expression of *rpoH*. For induction of *rpoH* in KH10, overnight cultures were selected for Tet and subsequently grown in LB absent for Tet. 1 hour prior to temperature shift for induction of Mu transposition, aTc was added. Genomic DNA was extracted with Wizards Genomic DNA Kit, and sequencing was performed by Novogene on NovaSeq PE150 platform. Partitioning of the genome into 100 bins was as described previously [8]. Data was processed using custom script described in [8] without LASSO regression. Instead, the number of insertions per bin was first corrected for total number of read counts, followed by correcting for replication effect by normalizing to the total number of *E. coli* reads mapped to that bin The average of three biological replicates and standard error was used to plot the data for normalized transposition frequency.

References

1. Gonzalez JM, Aranda B. Microbial Growth under Limiting Conditions-Future Perspectives. Microorganisms. 2023;11. doi:10.3390/microorganisms11071641

2. Bremer H, Dennis PP. Modulation of Chemical Composition and Other Parameters of the Cell at Different Exponential Growth Rates. EcoSal Plus. 2008;3. doi:10.1128/ecosal.5.2.3

3. Klappenbach JA, Dunbar JM, Schmidt TM. rRNA operon copy number reflects ecological strategies of bacteria. Appl Environ Microbiol. 2000;66: 1328–1333. doi:10.1128/AEM.66.4.1328-1333.2000

4. Fleurier S, Dapa T, Tenaillon O, Condon C, Matic I. rRNA operon multiplicity as a bacterial genome stability insurance policy. Nucleic Acids Res. 2022; 1–20. doi:10.1093/nar/gkac332

5. Condon C, Squires C, Squires CL. Control of rRNA transcription in Escherichia coli. Microbiol Rev. 1995;59: 623–645. doi:10.1128/mr.59.4.623-645.1995

6. Gaal T, Bratton BP, Sanchez-Vazquez P, Sliwicki A, Sliwicki K, Vegel A, et al. Colocalization of distant chromosomal loci in space in e. Coli: A bacterial nucleolus. Genes Dev. 2016;30: 2272–2285. doi:10.1101/gad.290312.116

7. Lioy VS, Cournac A, Marbouty M, Duigou S, Mozziconacci J, Espéli O, et al. Multiscale Structuring of the E. coli Chromosome by Nucleoid-Associated and Condensin Proteins. Cell. 2018;172: 771-783.e18. doi:10.1016/j.cell.2017.12.027

8. Walker DM, Freddolino PL, Harshey RM. A Well-Mixed E. coli Genome: Widespread Contacts Revealed by Tracking Mu Transposition. Cell. 2020;180: 703-716.e18. doi:10.1016/j.cell.2020.01.031

9. Walker DM, Harshey RM. Deep sequencing reveals new roles for MuB in transposition immunity and target-capture, and redefines the insular Ter region of E. coli. Mob DNA. 2020;11: 26. doi:10.1186/s13100-020-00217-9

10. Mercier R, Petit MA, Schbath S, Robin S, El Karoui M, Boccard F, et al. The MatP/matS Site-Specific System Organizes the Terminus Region of the E. coli Chromosome into a Macrodomain. Cell. 2008;135: 475–485. doi:10.1016/j.cell.2008.08.031

11. Celli J, Tsolis RM. Bacteria, the endoplasmic reticulum and the unfolded protein response: friends or foes? Nat Rev Microbiol. 2015;13: 71–82. doi:10.1038/nrmicro3393

12. Grossman AD, Erickson JW, Gross CA. The htpR gene product of E. coli is a sigma factor for heat-shock promoters. Cell. 1984;38: 383–390. doi:10.1016/0092-8674(84)90493-8

13. Nonaka G, Blankschien M, Herman C, Gross CA, Rhodius VA. Regulon and promoter analysis of the E. coli heat-shock factor, sigma32, reveals a multifaceted cellular response to heat stress. Genes Dev. 2006;20: 1776–1789. doi:10.1101/gad.1428206

14. John J, Jabbar J, Badjatia N, Rossi MJ, Lai WKM, Pugh BF. Genome-wide promoter assembly in E. coli measured at single-base resolution. Genome Res. 2022;32: 878–892. doi:10.1101/gr.276544.121

15. Nielsen HJ, Ottesen JR, Youngren B, Austin SJ, Hansen FG. The Escherichia coli chromosome is organized with the left and right chromosome arms in separate cell halves. Mol Microbiol. 2006;62: 331–338. doi:10.1111/j.1365-2958.2006.05346.x

16. Tosa T, Pizer LI. Biochemical bases for the antimetabolite action of L-serine hydroxamate. J Bacteriol. 1971;106: 972–982. doi:10.1128/jb.106.3.972-982.1971

17. Gourse RL, Chen AY, Gopalkrishnan S, Sanchez-Vazquez P, Myers A, Ross W. Transcriptional Responses to ppGpp and DksA. Annu Rev Microbiol. 2018;72: 163–184. doi:10.1146/annurev-micro-090817-062444

18. Zhang Y, Gross CA. Cold Shock Response in Bacteria. Annu Rev Genet. 2021;55: 377–400. doi:10.1146/annurev-genet-071819-031654

19. Cao H, Wei D, Yang Y, Shang Y, Li G, Zhou Y, et al. Systems-level understanding of ethanol-induced stresses and adaptation in E. coli. Sci Rep. 2017;7: 44150. doi:10.1038/srep44150

20. Macvanin M, Edgar R, Cui F, Trostel A, Zhurkin V, Adhya S. Noncoding rnas Binding to the Nucleoid Protein HU in Escherichia coli. J Bacteriol. 2012;194: 6046–6055. doi:10.1128/JB.00961-12

21. Ladouceur AM, Parmar BS, Biedzinski S, Wall J, Tope SG, Cohn D, et al. Clusters of bacterial RNA polymerase are biomolecular condensates that assemble through liquid-liquid phase separation. Proc Natl Acad Sci U S A. 2020;117: 18540–18549. doi:10.1073/pnas.2005019117

22. Cui L, Vigouroux A, Rousset F, Varet H, Khanna V, Bikard D. A CRISPRi screen in E. coli reveals sequence-specific toxicity of dCas9. Nat Commun. 2018;9: 1912. doi:10.1038/s41467-018-04209-5

23. Lee C, Cox RM, Papoulas O, Horani A, Drew K, Devitt CC, et al. Functional partitioning of a liquid-like organelle during assembly of axonemal dyneins. Carter AP, Akhmanova A, Stearns T, Kikkawa M, editors. Elife. 2020;9: e58662. doi:10.7554/eLife.58662

24. Yang D, Ye X, Lorimer GH. Symmetric GroEL: GroES2 complexes are the protein-folding functional form of the chaperonin nanomachine. Proc Natl Acad Sci U S A. 2013;110. doi:10.1073/pnas.1318862110

25. Fayet O, Ziegelhoffer T, Georgopoulos C. The groES and groEL heat shock gene products of Escherichia coli are essential for bacterial growth at all temperatures. J Bacteriol. 1989;171: 1379–1385. doi:10.1128/jb.171.3.1379-1385.1989

26. Cowing DW, Bardwellt JCA, Craigt EA, Woolfordt C, Hendrixt RW, Gross CA. Consensus sequence for Escherichia coli heat shock gene promoters (transcription initiation/ar factors/dnaK regulon). Proc Nati Acad Sci USA. 1985. Available: https://www.pnas.org

27. Guisbert E, Herman C, Lu CZ, Gross CA. A chaperone network controls the heat shock response in E. coli. Genes Dev. 2004;18: 2812–2821. doi:10.1101/gad.1219204

28. Lim B, Miyazaki R, Neher S, Siegele DA, Ito K, Walter P, et al. Heat shock transcription factor σ32 co-opts the signal recognition particle to regulate protein homeostasis in E. coli. PLoS Biol. 2013;11: e1001735. doi:10.1371/journal.pbio.1001735

29. Yura T, Guisbert E, Poritz M, Lu CZ, Campbell E, Gross CA. Analysis of \&\#x3c3;^{32} mutants defective in chaperone-mediated feedback control reveals unexpected complexity of the heat shock response. Proceedings of the National Academy of Sciences. 2007;104: 17638–17643. doi:10.1073/pnas.0708819104

30. Maeda H, Fujita N, Ishihama A. Competition among seven Escherichia coli σ subunits: relative binding affinities to the core RNA polymerase. Nucleic Acids Res. 2000;28: 3497–3503. doi:10.1093/nar/28.18.3497

31. Ishihama A. Functional Modulation of Escherichia Coli RNA Polymerase. Annu Rev Microbiol. 2000;54: 499–518. doi:10.1146/annurev.micro.54.1.499

32. Joo DM, Nolte A, Calendar R, Zhou YN, Jin DJ. Multiple regions on the Escherichia coli heat shock transcription factor sigma32 determine core RNA polymerase binding specificity. J Bacteriol. 1998;180: 1095–1102. doi:10.1128/JB.180.5.1095-1102.1998

33. Harshey RM. Transposable Phage Mu. 2014. doi:10.1128/microbiolspec

34. Belton J-M, McCord RP, Gibcus JH, Naumova N, Zhan Y, Dekker J. Hi-C: a comprehensive technique to capture the conformation of genomes. Methods. 2012;58: 268–276. doi:10.1016/j.ymeth.2012.05.001

35. Mcstay B. The p-Arms of Human Acrocentric Chromosomes Play by a Different Set of Rules. Annual Review of Genomics and Human Genetics Annu Rev Genom Hum Genet 2023. 2024;24: 48. doi:10.1146/annurev-genom-101122

36. Sochorová J, Gálvez F, Matyášek R, Garcia S, Kovařík A. Analyses of the updated “animal rdna loci database” with an emphasis on its new features. Int J Mol Sci. 2021;22. doi:10.3390/ijms222111403

37. Tsuneaki A, Ciarán C, Justina V, Dmitry Z, Binghua S, Michaal A-O, et al. Construction and Initial Characterization of Escherichia coli Strains with Few or No Intact Chromosomal rRNA Operons. J Bacteriol. 1999;181: 3803–3809. doi:10.1128/jb.181.12.3803-3809.1999

38. Campbell EA, Korzheva N, Mustaev A, Murakami K, Nair S, Goldfarb A, et al. Structural Mechanism for Rifampicin Inhibition of Bacterial RNA. Cell. 2001.

39. Dash S, Lamb MC, Lange JJ, McKinney MC, Tsuchiya D, Guo F, et al. rRNA transcription is integral to phase separation and maintenance of nucleolar structure. PLoS Genet. 2023;19. doi:10.1371/journal.pgen.1010854

40. Enz S, Braun V, Crosa JH. Transcription of the region encoding the ferric dicitrate-transport system in Escherichia coli: similarity between promoters for fecA and for extracytoplasmic function sigma factors. Gene. 1995;163: 13–18. doi:10.1016/0378-1119(95)00380-o

41. Enz S, Mahren S, Stroeher UH, Braun V. Surface signaling in ferric citrate transport gene induction: interaction of the FecA, FecR, and FecI regulatory proteins. J Bacteriol. 2000;182: 637–646. doi:10.1128/JB.182.3.637-646.2000

42. Ferguson AD, Chakraborty R, Smith BS, Esser L, van der Helm D, Deisenhofer J. Structural Basis of Gating by the Outer Membrane Transporter FecA. Science (1979). 2002;295: 1715–1719. doi:10.1126/science.1067313

43. Susanne M, Volkmar B. The FecI Extracytoplasmic-Function Sigma Factor of Escherichia coli Interacts with the β' Subunit of RNA Polymerase. J Bacteriol. 2003;185: 1796–1802. doi:10.1128/jb.185.6.1796-1802.2003

44. Erickson JW, Gross CA. Identification of the sigma E subunit of Escherichia coli RNA polymerase: a second alternate sigma factor involved in high-temperature gene expression. Genes Dev. 1989;3: 1462–1471. doi:10.1101/gad.3.9.1462

45. Missiakas D, Raina S. The extracytoplasmic function sigma factors: role and regulation. Mol Microbiol. 1998;28: 1059–1066. doi:10.1046/j.1365-2958.1998.00865.x

46. Missiakas D, Mayer MP, Lemaire M, Georgopoulos C, Raina S. Modulation of the Escherichia coliσE (RpoE) heat-shock transcription-factor activity by the RseA, RseB and RseC proteins. Mol Microbiol. 1997;24: 355–371. doi:https://doi.org/10.1046/j.1365-2958.1997.3601713.x

47. Campbell EA, Tupy JL, Gruber TM, Wang S, Sharp MM, Gross CA, et al. Crystal Structure of Escherichia coli σE with the Cytoplasmic Domain of Its Anti-σ RseA. Mol Cell. 2003;11: 1067–1078. doi:https://doi.org/10.1016/S1097-2765(03)00148-5

48. Kanehara K, Ito K, Akiyama Y. YaeL proteolysis of RseA is controlled by the PDZ domain of YaeL and a Gln-rich region of RseA. EMBO J. 2003;22: 6389–6398. doi:https://doi.org/10.1093/emboj/cdg602

49. Ades SE, Connolly LE, Alba BM, Gross CA. The Escherichia coli sigma(E)-dependent extracytoplasmic stress response is controlled by the regulated proteolysis of an anti-sigma factor. Genes Dev. 1999;13: 2449–2461. doi:10.1101/gad.13.18.2449

50. Ishihama A. Subunit of assembly of Escherichia coli RNA polymerase. Adv Biophys. 1981;14: 1–35.

51. Mathew R, Chatterji D. The evolving story of the omega subunit of bacterial RNA polymerase. Trends in Microbiology. 2006. pp. 450–455. doi:10.1016/j.tim.2006.08.002

52. Ross W, Gosink KK, Salomon J, Igarashi K, Zou C, Ishihama A, et al. A Third Recognition Element in Bacterial Promoters: DNA Binding by the α Subunit of RNA Polymerase. Science (1979). 1993;262: 1407–1413. doi:10.1126/science.8248780

673 53. Ziemienowicz A, Skowyra D, Zeilstra-Ryallsqli J, Fayet O, Georgopoulos C, Zylicz MY. The Journal
674 of Biological Chemistry. Both the Escherichia coli Chaperone Systems, GroEL/GroES and
675 DnaKIDnaJIGrpE, Can Reactivate Heat-treated RNA Polymerase. 1993.

676 54. Cabrera JE, Jin DJ. The distribution of RNA polymerase in Escherichia coli is dynamic and
677 sensitive to environmental cues. Mol Microbiol. 2003;50: 1493–1505. doi:10.1046/j.1365-
678 2958.2003.03805.x

679 55. Stracy M, Lesterlin C, Garza de Leon F, Uphoff S, Zawadzki P, Kapanidis AN. Live-cell
680 superresolution microscopy reveals the organization of RNA polymerase in the bacterial nucleoid.
681 Proc Natl Acad Sci U S A. 2015/07/29. 2015;112: E4390–E4399. doi:10.1073/pnas.1507592112

682 56. Jin DJ, Cagliero C, Zhou YN. Growth rate regulation in Escherichia coli. FEMS Microbiol Rev.
683 2012;36: 269–287. doi:10.1111/j.1574-6976.2011.00279.x

684 57. Weng X, Bohrer CH, Bettridge K, Lagda AC, Cagliero C, Jin DJ, et al. Spatial organization of RNA
685 polymerase and its relationship with transcription in Escherichia coli. Proceedings of the National
686 Academy of Sciences. 2019;116: 20115–20123. doi:10.1073/pnas.1903968116

687 58. Gibson DG, Young L, Chuang R-Y, Venter JC, Hutchison CA, Smith HO. Enzymatic assembly of DNA
688 molecules up to several hundred kilobases. Nat Methods. 2009;6: 343–345.
689 doi:10.1038/nmeth.1318

690 59. Datsenko KA, Wanner BL. One-step inactivation of chromosomal genes in *Escherichia coli* K-12
691 using PCR products. Proceedings of the National Academy of Sciences. 2000;97: 6640–6645.
692 doi:10.1073/pnas.120163297

693

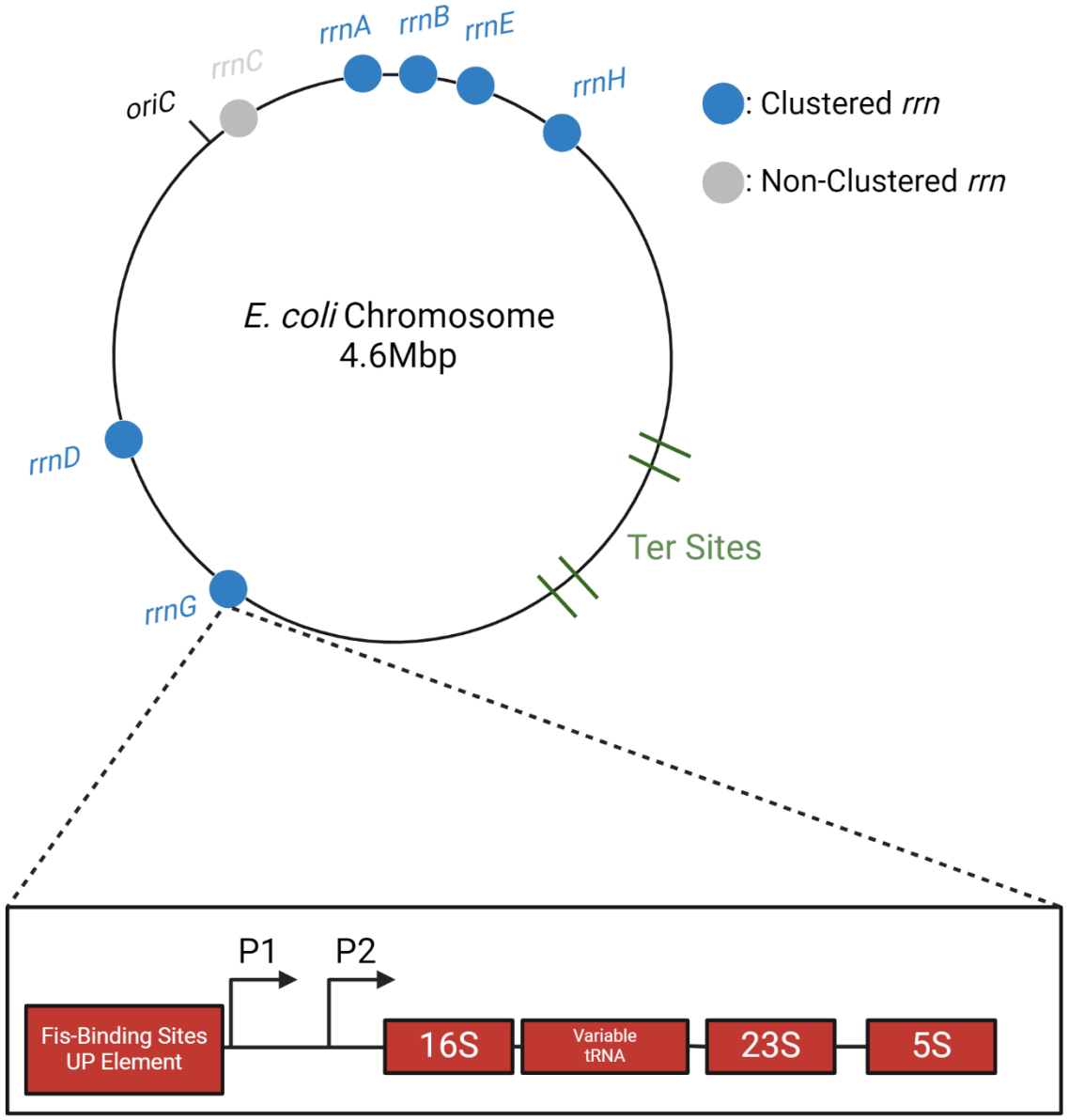

Fig. 1*:* Distribution of *rrn* operons on the *E. coli* genome. On the circular *E. coli* chromosome, replication originates at *oriC*, with two bidirectional replication forks traversing each arm (replicore), terminating within the Ter region. Locations of the *rrn* operons shown to cluster by two different methodologies (see text) are indicated by blue-filled circles. Organization of a typical *rrn* operon is shown for *rrnG*; P1 and P2 promoters are indicated by arrows.

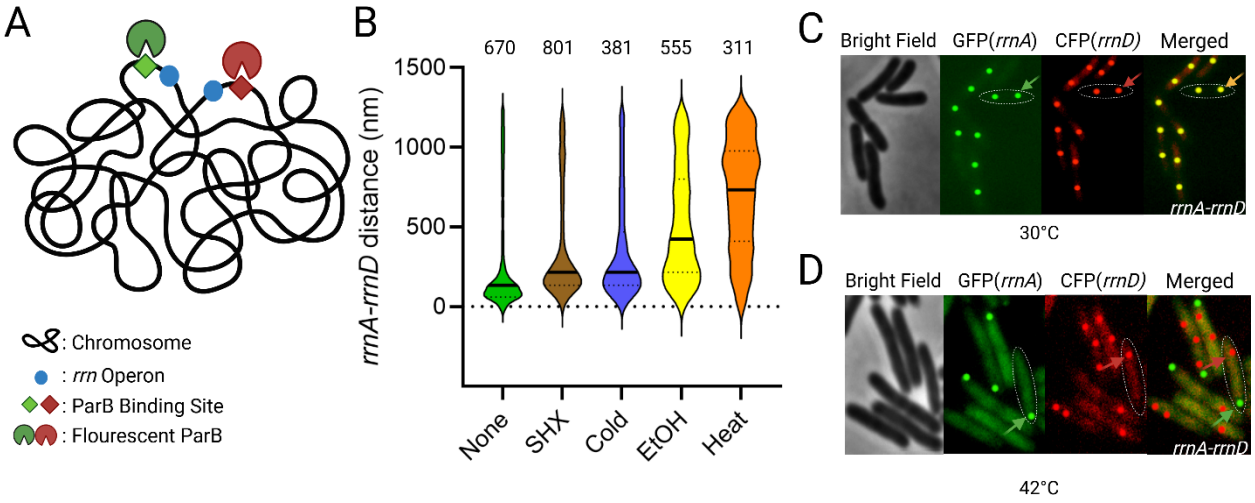

Fig. 2: Distance between *rrnA* and *rrnD* operons under various stress conditions. (A) Scheme for *rrn* operon tagging. Two different *par* sites (*parS*T1 and *parS*P1) were placed upstream of *rrnA* and *rrnD*, respectively, in the parent strain MG1655. These sites were visualized by co-expression of their cognate fluorescent ParB proteins (pMT1 GFP-ParB and P1 CFP-ParB). (B) Violin plots of the distance between *rrnA* and *rrnD* under indicated stress conditions (see Methods for details). The numbers on the top refer to *rrn* pairs observed for one of three biological replicates. The solid line indicates the median distance, and the top and bottom dashed lines indicate the 3rd and 1st quartile, respectively. We note that due to the large number of foci observed, a small change in the median distance is considered statistically significant ($p<0.001$) under Mann-Whitney test. We arbitrarily considered a 2-fold change of median distance to be significant. (C) Images used to generate data in (B). Representative image of *rrnA-rrnD* clustering without added stress. GFP and CFP were false-colored and enhanced for better visualization. One cell is outlined, with an arrow pointing to a merged GFP/CFP focus. The foci are edited in post-processing as a perfect circle to provide better contrast and visualization. Most cells appear to contain 2 copies of the *rrn* operons, indicating that this region of the chromosome is replicated. (D) Representative image of *rrnA-rrnD* de-clustering with heat stress. Colored arrows indicate focus from either GFP-field (green) or CFP (red). We note that the number of *rrnA*-GFP foci is reduced to 1 focus per cell.

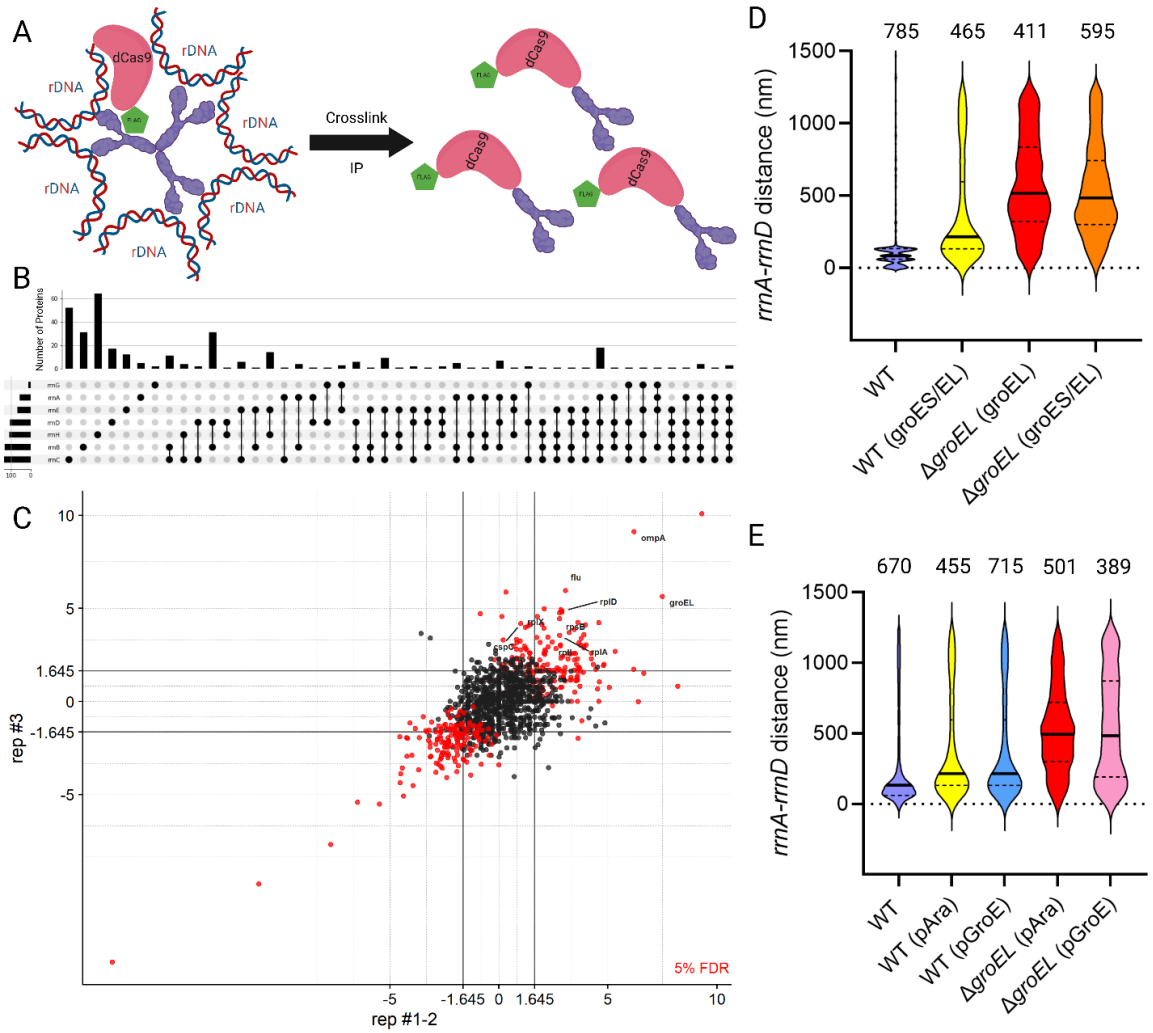

Fig. 3: Deregulation of GroEL disrupts *rrnA-rrnD* clustering. (A) Scheme for pulldown of proteins in the vicinity of all *rrn* loci. dCas9-FLAG (pink/green) was directed upstream of all 7 *rrn* loci by expressing sgRNA specific for each target. Formaldehyde was used to crosslink dCas9 to putative bridging factor(s) (purple). The dCas9-linked 'complex' was then immunoprecipitated and subjected to mass spectrometry (MS). (B) Aggregated MS results of significantly enriched proteins from dCas9 pulldown. The bar graph shows the number of proteins identified for each combination. The black ball indicates the pulldown of the sgRNA of interest, and the black line connecting them indicates co-occurrence of the proteins in the indicated sgRNA pulldowns. (C) Significantly enriched proteins in pulldown with gRNA targeting *yeiP* (*rrnC*). Each protein is identified by a circle. Each axis represents the z-score of each protein in separate experiments. Lines from the axes indicate the cut-off for enrichment. Red circles and black circles indicate proteins that fall above and below the False Discovery Rate (FDR) (5%), respectively. Proteins significantly enriched are in the top-right square (z score>2.5) with the protein name in red. See Fig. S4 for data obtained for the remaining gRNAs. (D) Distance between *rrnA-D* operons in WT and Δ*groEL* strains expressing either both *groES/groEL* or *groEL* alone from pAraBAD plasmid. Other descriptions as in Fig. 2. (E) Distance between *rrnA-D* in WT and Δ*groEL* strains expressing *groES/groEL* from either pAra or the native *groE* promoter.

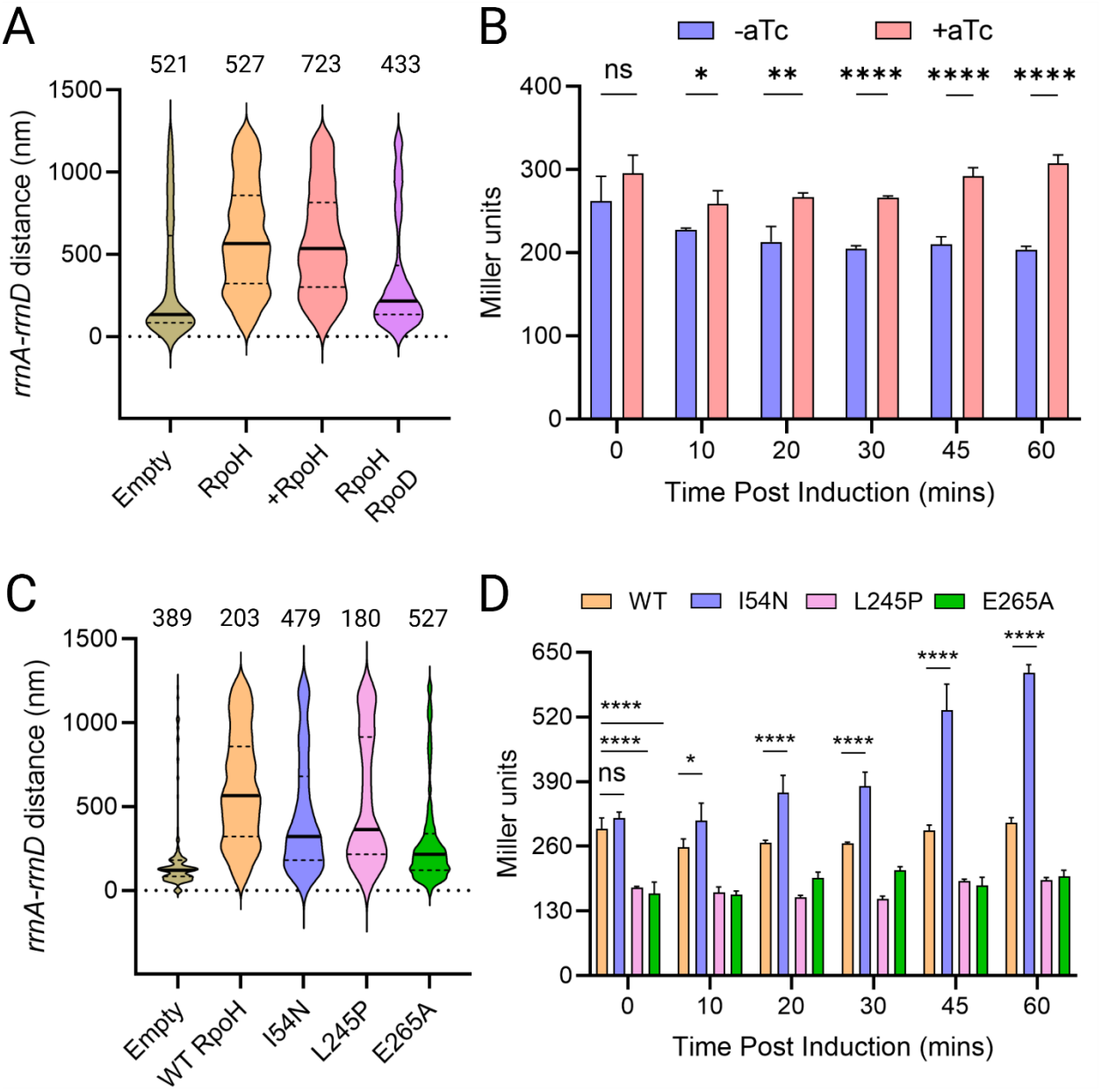

Figure 4: **σ^H promotes de-clustering of *rrnA-rrnD* independent of its transcriptional activity**
(A) Distance between *rrnA-D* with ectopic expression of *rpoH* from pTc. Induction was carried out for one hour prior to microscopy. In the 4th plot from left, RpoD is cloned downstream of TetR, from a constitutively expressed promoter, divergent from pTc. All other descriptions as in Fig. 2. (B) Transcriptional activity of ectopically expressed *rpoH*. Miller assay was carried out as described in Methods. Student t's test was performed pairwise to determine statistical significance (two tailed, ns: not statistically significant, *: p<0.05, **: p< 0.01, ****: p< 0.0001). (C) Distance between *rrnA-D* with ectopic expression of indicated *rpoH* mutants, compared to empty vector control. (D) Transcriptional activity of ectopically expressed *rpoH* mutants, as described in B.

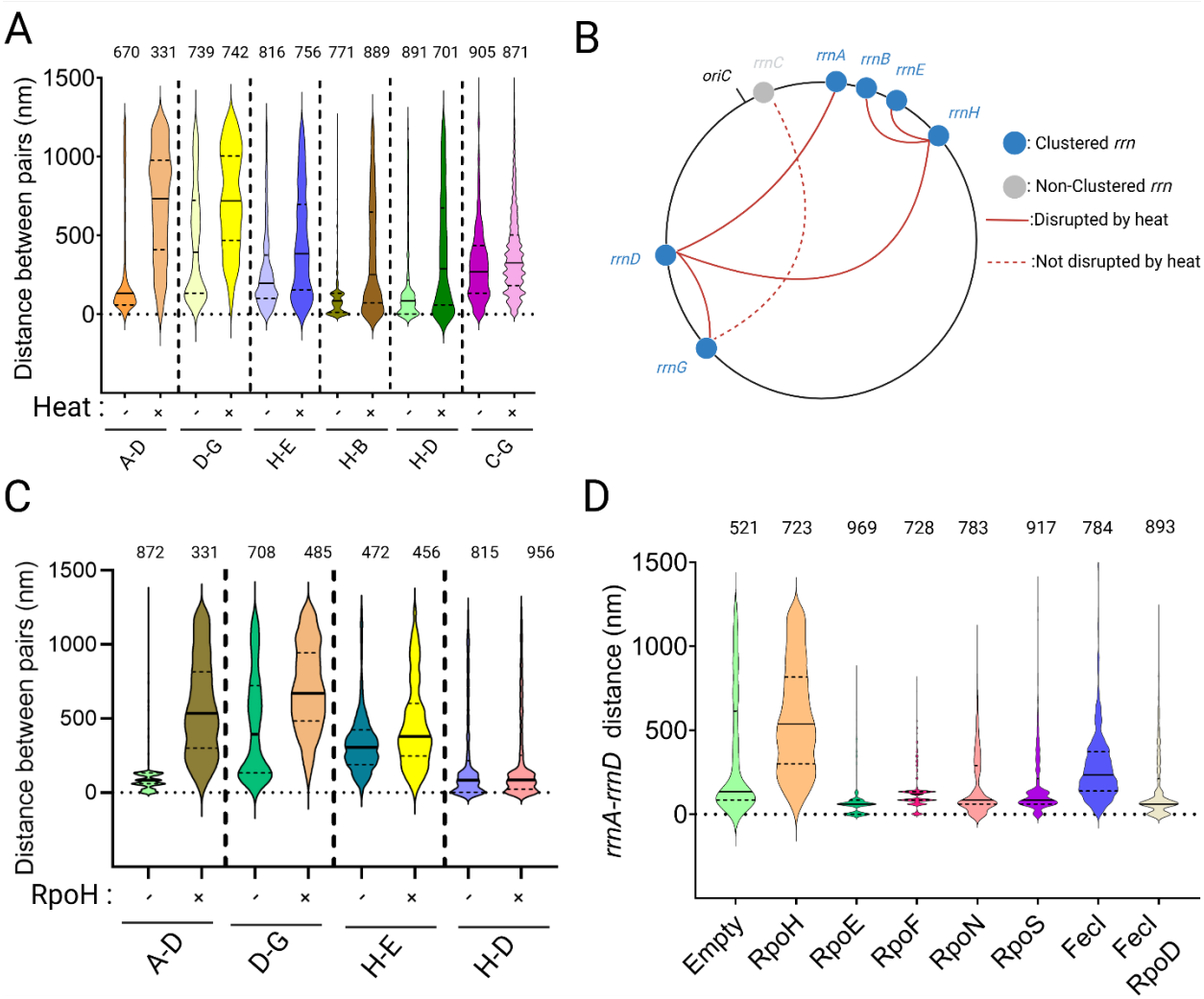

Figure 5: Disruption of *rrn* clustering by heat stress and by FecI. (A) Effect of heat stress on clustering of *rrn* pairs. Other descriptions as in Fig. 2. (B) Response to heat stress of tested *rrn* pairs. Each of the 7 *rrn* operons was visited at least once. (C) Response to *rpoH* induction of tested *rrn* pairs. (D) Effect of ectopic expression of five σ factors on clustering *rrnA-D*, all placed under control of pTc with the same RBS. +/- symbols are self-explanatory.

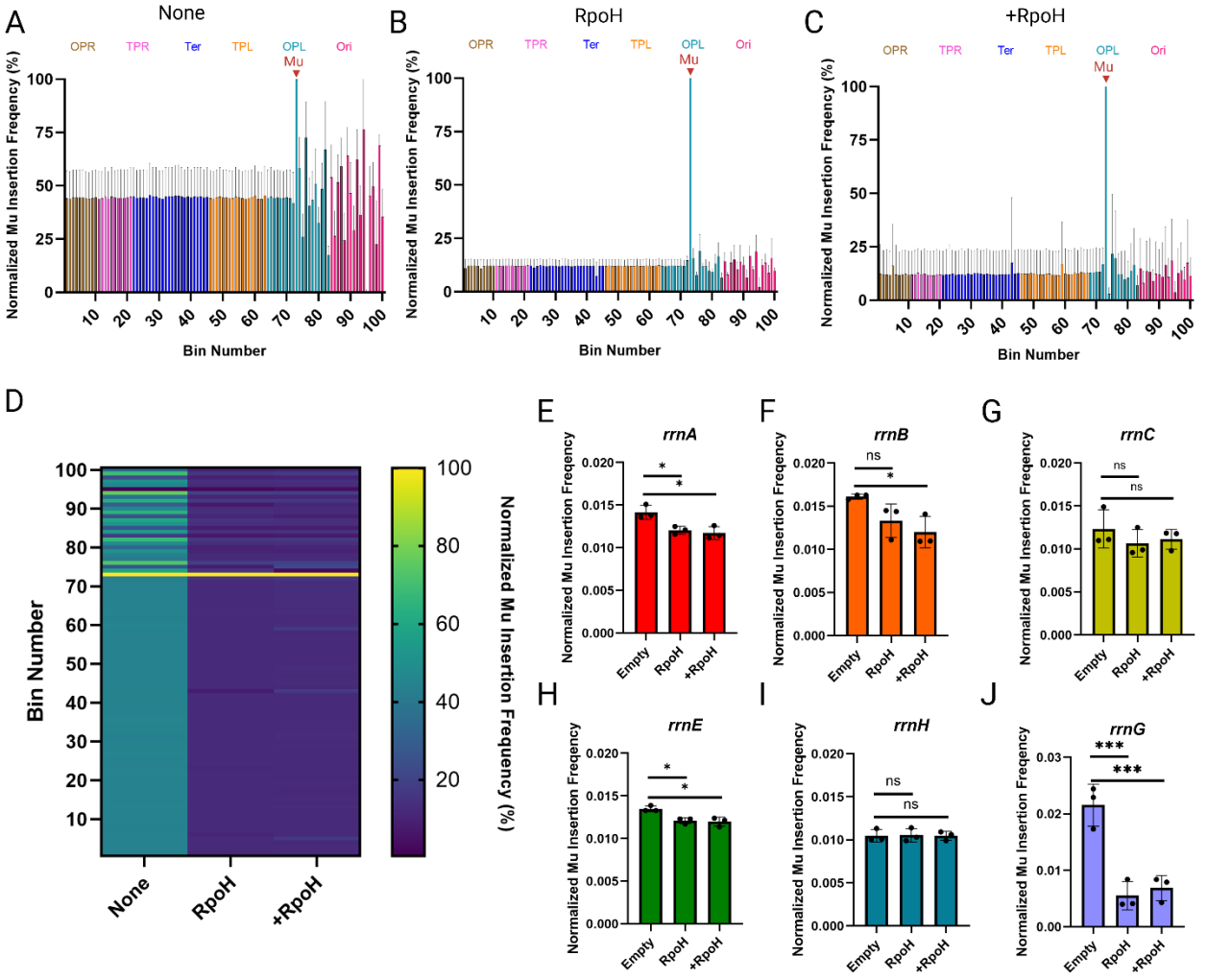

Figure 6: Expression of *rpoH* promotes local chromosomal contacts. (A) Frequency of transposition of Mu located in the vicinity of *rrnD* (Bin 72) after one round of transposition. The number of insertions has been normalized to the read depth of each bin. The initial Mu position is indicated by a red triangle. The *E. coli* genome was partitioned into 100 equally sized bins, so each bin is ~46 kb. Starting Bin #s and chromosomal regions are indicated on top. Each vertical bar represents the average normalized transposition frequency of 3 biological replicates at the indicated bin, expressed as a percentage (with the highest transposition frequency being set to 100%). Grey error bars are the standard deviation. Color bars indicate regions of the *E. coli* chromosome annotated up top. (B) Same as (A) but with the *rpoH* overexpression vector. (C) Same as (B) but with induction of *rpoH* expression. (D). Heat map of the data from A through C. (E-J). Transposition frequency from *mlaF* (*rrnD*) into the indicated *rrn* operon-containing bin under conditions described in A through C. The individual data points and associated standard deviation are shown. Statistical significance was determined with Student t's test (two-tailed), *: p<0.05. ns: not statistically significant.

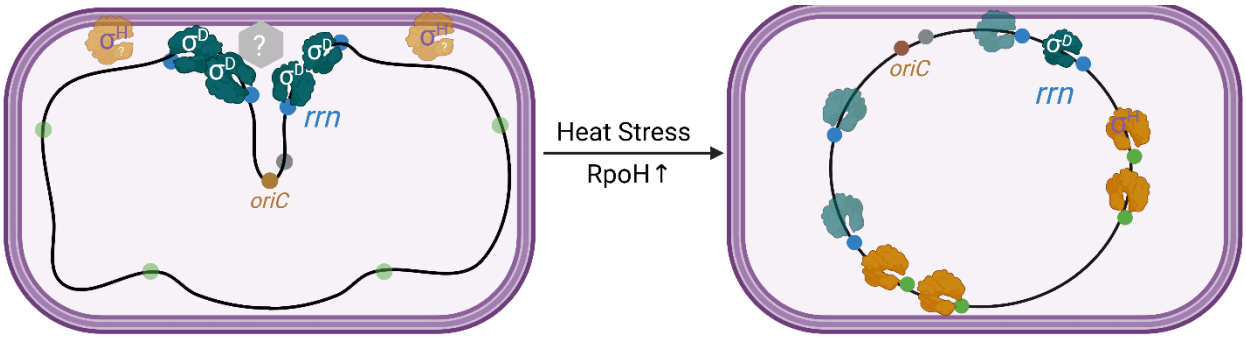

Figure 7: Model for *rrn* clustering mediated by σ^D. Left: Clustering of *rrn* operons is mediated by σ^D at the membrane either through σ^D directly or through other unknown factor(s) (grey hexagon). Upon heat stress or elevated σ^H levels, RNAP complexes (dark green) bound to σ^D transcribing the *rrn* operons (blue circles) are displaced through competition with σ^H, which is typically localized to the inner membrane and degraded. RNAP-core complexed with σ^H (orange) transcribes genes in σ^H regulon (green circles), lowering the total amount of RNAP transcribing *rrn* operons at the membrane, resulting in their de-clustering.